This is the author's version of an article that has been published in this journal. Changes were made to this version by the publisher prior to publication.
The final version of record is available at http://dx.doi.org/10.1109/TPWRS.2018.2890296

Stability-Constrained Adaptive Droop for Power Sharing in AC-MTDC Grids

Amirthagunaraj Yogarathinam, *Student Member, IEEE*, and Nilanjan Ray Chaudhuri, *Senior Member, IEEE*

***Abstract*—A secure operation of AC-MTDC grids following an (N-1) contingency (e.g. converter outage), is of a major concern for the system planners and operators. For the case of converter outage, the concept of adaptive droop control enables the healthy converters to share the burden of power mismatch in an effective manner. However, certain settings of the droop coefficients may lead to instability of the AC grid where multiple converters are connected and one of them goes out. This paper proposes a stability-constrained adaptive droop approach for autonomous power sharing following the outage of a converter in an MTDC grid. A Trajectory Sensitivity Analysis (TSA)-based approach is presented to impose the constraints on the adaptive droop gains, which can be an outcome of Dynamic Security Assessment (DSA) performed by the system operators. The robustness of the proposed approach for post-contingency system is demonstrated through nonlinear time-domain simulation results using models developed in MATLAB/Simulink.**

***Index Terms*—Adaptive Droop, Dynamic Security Assessment (DSA), Multiterminal DC (MTDC) Grids, Power Sharing, Trajectory Sensitivity Analysis, Voltage Source Converter (VSC).**

I. Introduction

With a significant increase in the penetration of renewable energy in modern power grid, a substantial research attention has been focused on multiterminal DC (MTDC) grids, which typically include voltage-source converter high-voltage DC (VSC-HVDC) transmission systems [1]. Similar to the AC grids, a secure operation of AC-MTDC grids following a single-point failure i.e. an (N-1) contingency, is of a major concern for the system planners and operators. The focus of this paper is the secure operation of such systems following a converter outage.

In literature, the concept of droop control has been proposed to share the burden of power mismatch among the healthy converters following such a contingency [2]–[4]. In the primary level, a fixed predetermined voltage-current or voltage-power droop characteristic has been used, which is based on the individual ratings of the converters. When a fixed set of droop coefficients are used, system planners can perform offline planning studies to ensure that the AC-MTDC grid is secure following a converter outage.

As opposed to the fixed droop constants, in [5] the authors have proposed an adaptive droop control scheme for appropriate power sharing by taking into account the available headrooms of the converters to avoid possible overloading. The idea of adaptive droop has gained popularity in the areas of MTDC [6]–[17] and microgrids [18], [19] among others [20]. In [6]–[8], the droop coefficients of the MTDC grid were designed based on a DC optimal power flow (OPF). In [9], the adaptive droop controller is implemented by considering the effect of the DC cable dynamics. Marten $et\ al$ in [10], proposed a new $p-v$ characteristic-based adaptive control for local DC-nodes to meet the grid requirements. In [11], an adaptive droop is proposed to support hierarchical control strategy for MTDC networks with large-scale penetration of renewable energy and battery storage. A Model Predictive Control (MPC)-based coordinating droop controller for MTDC grid is proposed in [12]. An adaptive droop DC-bus voltage controller for grid-connected VSC with an LCL output filter in renewable energy application is presented in [20] and the optimized adaptive droop schemes are used for MTDC grid connected to offshore wind farms in [13], [14]. In [15], the adaptive droop coefficient for power sharing in MTDC grid is calculated based on the AC grid frequency, whereas in [16], available power headrooms and voltage rating of the converters are considered, which is an extended version of the one proposed in [5].

Although, the concept of adaptive droop control has been applied in MTDC grids, none of [6]–[16] have considered the stability constraints of the droop coefficients. A few papers [17], [21]–[23] have tried to address this issue. A fuzzy logic-based adaptive droop controller utilizing the available power capacity of the converters is proposed in [17]. In [21] an accurate power sharing control scheme is proposed using the communication of Power Sharing Index (PSI) between the neighboring converters. References [17] and [21] analyzed the stability of the system with variation in the droop coefficients using the traditional small-signal analysis.

Thams $et-al$ in [22] have studied the effectiveness of different droop controllers using the Active Power Transfer Capability (APTC). A methodology is also proposed to identify the acceptable operating points of the system based on voltage and current limits, damping ratios of the eigenvalues, and maximum DC voltage deviation using the linearized model of the system. References [17], [21], and [22] did not consider the dynamic model of the AC system connected to the MTDC grid. In [23], the effect of converter outage on the AC system dynamics of an AC-MTDC grid is analyzed using Singular Value Decomposition (SVD) based on the linearized model of the system, which builds on the SVD-based method originally proposed in [24] to analyze the DC-side dynamics of an MTDC grid.

When the droop constants are varied online as proposed in [6]–[14], [17], it is imperative to ascertain the region

The authors are with the School of Electrical Engineering & Computer Science, The Pennsylvania State University, University Park, PA 16802, USA (e-mail: *axy43@psu.edu, nuc88@engr.psu.edu*).

Financial support from NSF Grant Award ECCS 1656983 is gratefully acknowledged.

Copyright (c) 2019 IEEE. Personal use is permitted. For any other purposes, permission must be obtained from the IEEE by emailing pubs-permissions@ieee.org.

This is the author's version of an article that has been published in this journal. Changes were made to this version by the publisher prior to publication.
The final version of record is available at http://dx.doi.org/10.1109/TPWRS.2018.2890296

of stability in the multi-dimensional droop coefficient space. Although [17], [21]–[23] are significantly important in understanding the impact of droop constants on system stability, they have the following limitations -

1. References [17], [21], and [22] used eigenvalue analysis that did not take into account converter outage. Reference [23] modeled converter outage using a disturbance transfer function and relied on SVD-based analysis rooted in linear control theory. Scope of such analysis is limitted to oscillatory instability problem - not the first swing stability issue stemming from lack of synchronizing torque.
2. More importantly, following a converter outage, the nonlinearity and nonsmooth nature of system response becomes significantly pronounced due to large transients, limit hitting in converter controls, and other regulators in the AC system. Therefore, the validity of linear control theory (e.g. eigenvalue analysis, SVD, etc.)-based stability constraints become questionable.

We pose the problem at hand as the so-called Dynamic Security Assessment (DSA) problem where the goal is to determine the stability constraints of the adaptive droop coefficients following a converter outage (i.e. N-1) contingency. Trajectory Sensitivity Analysis (TSA) has been applied for DSA of traditional AC system [25] - we propose to extend this approach for the AC-MTDC grid to determine these stability constraints.

TSA works based upon linearization of the system around trajectories rather than an equilibrium point [25]–[27]. The distinct advantages of TSA are: (a) it enables determination of parametric influence on the nonlinear and nonsmooth behavior of a power system [25]–[27], (b) it is not limited by the complexity of the model, and (c) the computational overload is minimized if implicit integration techniques are used [26]. As the system becomes more stressed, the sensitivity of the state trajectories with respect to parameters increases significantly, which can be used to determine the stability constraints of the parameters [25]. We propose to apply this property for evaluating the region of stability in the multi-dimensional droop coefficient plane following the converter outage.

The paper is organized as follows: following this introductory section, Section II briefly touches upon the modeling of the AC-MTDC grid. Autonomous power sharing using the adaptive droop approach is introduced in Section III. Section IV presents the proposed stability-constrained adaptive droop approach. The nonlinear time-domain simulation results of the study system developed in MATLAB/Simulink are discussed in Section V. Finally, Section VI concludes the paper.

II. Model of AC-MTDC Grid

Figure 1 shows the study system used in this paper, which includes three asynchronous AC systems connected to a 4-terminal bipolar MTDC grid with metallic return network where converter station #1 has its mid-point grounded with a resistance. The test system data can be found in [28].
The modeling philosophy of the AC and the DC grids are well-reported in literature – a very brief description is included here for the sake of completeness of this paper.

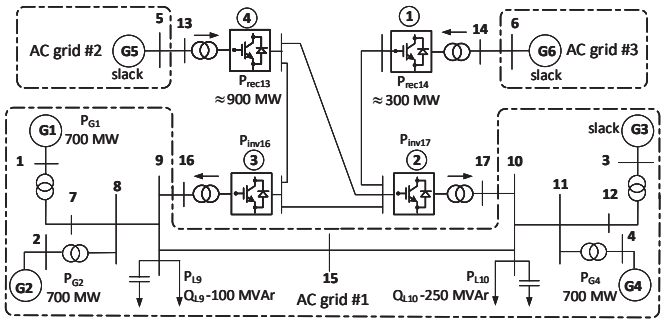

Fig. 1. Single-line diagram of the test system: Asymmetric bipole MTDC grid connected to three asynchronous AC systems.

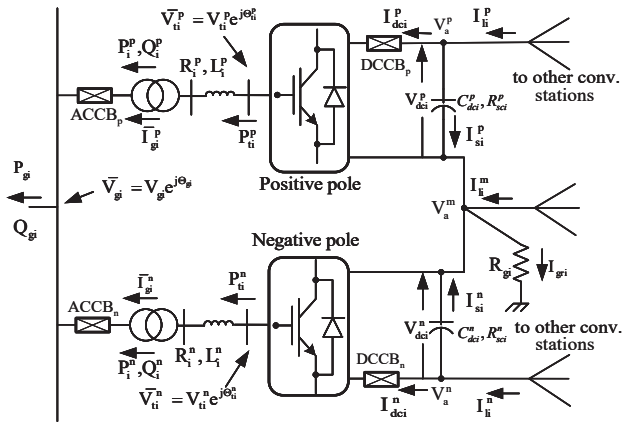

Fig. 2. Schematic of i^{th} converter station of the MTDC grid. To simulate the outage of any converter pole (positive or negative), the respective AC and DC side circuit breakers (ACCB and DCCB) are opened.

A. AC Grid Model

The AC systems are modeled in a fundamental frequency phasor framework. The models of its components are summarized below.

Generator Model: As shown in Fig. 1, there are 6 synchronous generators (SGs) (G1-G6) in the AC grids connected to the MTDC system. The SGs are represented by sixth-order sub-transient model [29] in synchronously rotating $d-q$ reference frame. Each SG is equipped with an IEEE-DC1A exciter [30] and a governor.

Load Model: The loads are represented by static models where the real part is of constant current type and the reactive part is of constant impedance type.

AC Network Model: The AC network is modeled algebraically using a Y -bus matrix in a current injection framework.

B. MTDC Grid Model

Converter Model: The positive and negative poles of the converter stations (Fig. 2) are represented by averaged models of a two-level converter in a synchronously rotating $d-q$ reference frame [31]. Traditional vector control with inner current control loops are considered [32]. To achieve decoupled control of active and reactive power, the $d-q$ reference frame is synchronized with the voltage space phasor $\bar{V}_{gi}$.

Copyright (c) 2019 IEEE. Personal use is permitted. For any other purposes, permission must be obtained from the IEEE by emailing pubs-permissions@ieee.org.

This is the author's version of an article that has been published in this journal. Changes were made to this version by the publisher prior to publication.
The final version of record is available at http://dx.doi.org/10.1109/TPWRS.2018.2890296

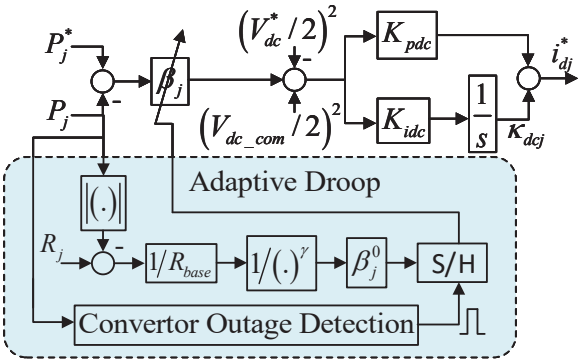

Fig. 3. $P - V_{dc}$ adaptive droop control in the j^{th} converter. β_j and κ_{dcj} are the droop coefficient and DC voltage controller state, respectively.

In this study, the active power channel of the converters are operated in $P - V_{dc}$ droop control with common DC-link voltage [28], see Fig. 3, whereas the reactive power channel maintains unity power factor at the PCC. The DC bus of converter station #1 is used for measuring the common DC voltage V_{dc-com}. The details of converter model and control structure can be found in [28]. The concept of adaptive droop coefficient will be explained later.

DC Network Model: The bipolar MTDC transmission network consists of cables forming positive, negative and metallic return paths. Unless otherwise mentioned, in this work the DC cable is represented by a single π-section model as in [28].

III. Converter Outage: Autonomous Power Sharing with Adaptive Droop

Converter outage is one of the most severe (N-1) contingencies in the AC-MTDC grid. Following such an outage, it is desirable to share the burden of the lost converter among the remaining ones, which can be achieved by the $P - V_{dc}$-based droop control using a common DC voltage shown in Fig. 3.

Reference [5] proposed an adaptive droop scheme for MTDC grids to share the power imbalance according to the available headroom of the power converters, which is the focus of this paper. The headroom H_j for the j^{th} converter is the difference between its rating R_j and the present loading P_j. The droop coefficient is computed based on the following relationship:

$$\beta_j = \beta_j^0 \left(\frac{R_{base}}{H_j} \right)^{\gamma} \tag{1}$$

where, β_j^0 is the nominal droop proportional to the rating R_j, R_{base} is the maximum value of all the converter ratings, and and γ is a positive constant. This ensures that the converter with less available headroom will share less burden. The implementation of this scheme is shown in Fig. 3. This method initially uses the values of droop coefficients calculated based on the pre-contingency steady-state following the converter outage in the immediate past. It keeps calculating the available headroom-dependent droop coefficients, but does not use them till the next converter outage. Upon detection of a converter outage, a sample and hold function is used to update the droop coefficients. This approach is shown inside the dotted box in Fig. 4(a).

Although the adaptive droop control is proven to be useful for avoiding converter overloading, certain combinations of droop constants can make the system unstable - a problem acknowledged in [5]. To solve this, we propose a stability-constrained adaptive droop scheme for system planners and operators, which is described next.

IV. Proposed Stability-Constrained Adaptive Droop

To ensure (N-1) contingency-secure operation, the system operators need to perform a Dynamic Security Assessment (DSA) [25], which is essentially a *'what if'* analysis at a certain operating point for probable converter outages. The goal is to proactively establish stability constraints for the droop gains, which is challenging due to the following reasons -

1. Since the converter outage is one of the most critical (N-1) contingencies, it leads to significant nonlinearity in response and converter controllers inevitably hit certain limits. Therefore, linear analysis-based approaches like eigenvalue-based [17], [21], [22] or singular value-based [23] methods have limited theoretical justifications.
2. Operators will need to obtain the constraints within a reasonable time frame. Therefore, it will be impossible to determine them purely based on numerous time-domain simulations.

In this paper, we propose a Trajectory Sensitivity Analysis (TSA)-based approach to determine a) the stability constraints for system operators, see Fig. 4(b), and b) a stability region for system planners, see Fig. 4(c). The proposed approach is described in detail in the following subsections.

A. Proposed Approach

TSA is a theoretically robust approach based upon linearization of the system around a trajectory rather than around an equilibrium point [25], which can analyze the influence of parameters on the nonlinear and non-smooth response trajectories manifested by the AC-MTDC grid following a converter outage.

1) Trajectory Sensitivity Analysis (TSA): The TSA can provide some valuable insights into the system responses due to parameter changes with the expense of a negligible amount of extra computation. A large trajectory sensitivity implies that the parameter significantly influences the system behavior [25]–[27].

With the state variable vector $\boldsymbol{x}$, the algebraic variable vector $\boldsymbol{z}$, and the vector of system parameters that are subject to change $\boldsymbol{\lambda}$, the AC-MTDC grid can be represented using the following Differential and Algebraic Equations (DAEs):

$$\dot{\boldsymbol{x}} = \boldsymbol{F}(\boldsymbol{x}, \boldsymbol{z}, \boldsymbol{\lambda}) \qquad \boldsymbol{x}(t_0) = \boldsymbol{x}_0 \tag{2}$$

$$\boldsymbol{0} = \boldsymbol{G}(\boldsymbol{x}, \boldsymbol{z}, \boldsymbol{\lambda}) \qquad \boldsymbol{z}(t_0) = \boldsymbol{z}_0 \tag{3}$$

For example, the converter droop coefficients $\boldsymbol{\beta}$, which change adaptively following a converter outage can be considered as

Copyright (c) 2019 IEEE. Personal use is permitted. For any other purposes, permission must be obtained from the IEEE by emailing pubs-permissions@ieee.org.

This is the author's version of an article that has been published in this journal. Changes were made to this version by the publisher prior to publication.
The final version of record is available at http://dx.doi.org/10.1109/TPWRS.2018.2890296

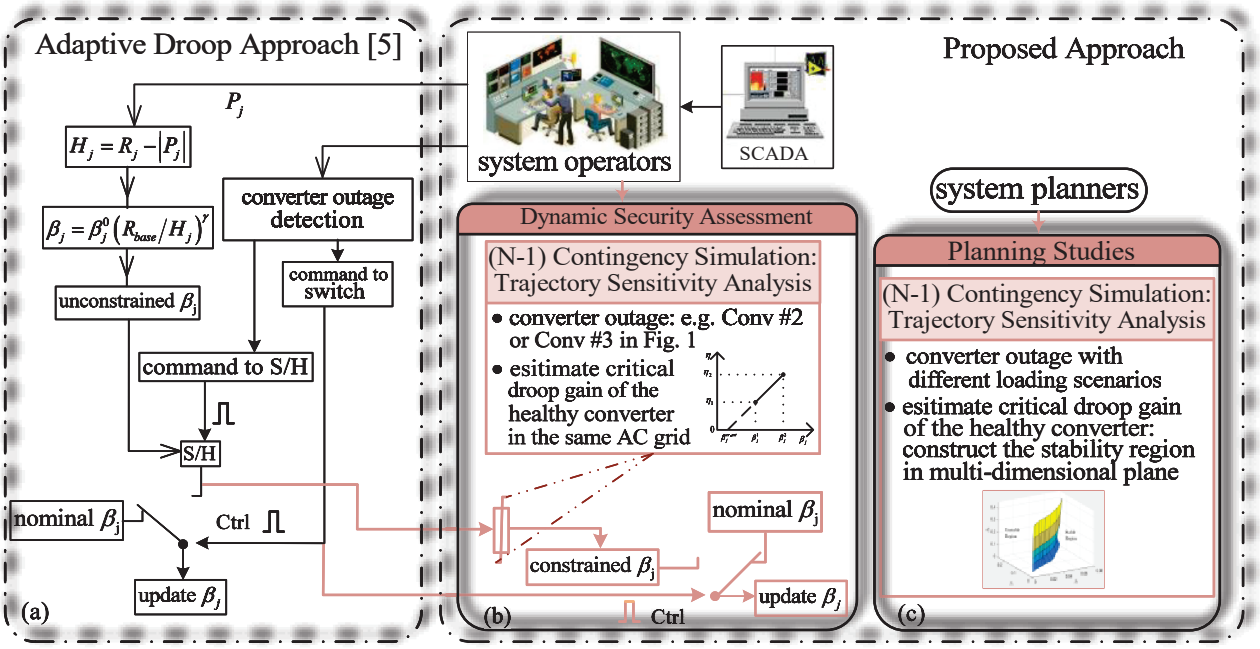

Fig. 4. (a) The adaptive droop approach [5]. The proposed Trajectory Sensitivity Analysis (TSA)-based approach to determine (b) the stability constraints for system operators and (c) a stability region for system planners that can be used as an operating guide.

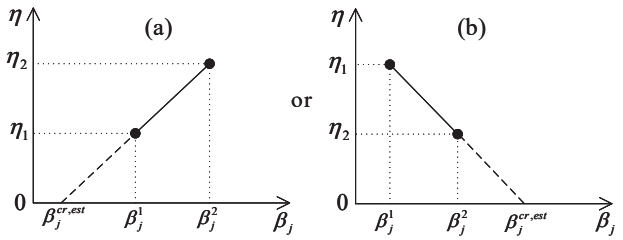

Fig. 5. Estimate of critical value of β from η versus β curve: (a) when β_j^{cr} appears as a lower limit. (b) when β_j^{cr} appears as an upper limit.

the parameter vector $\boldsymbol{\lambda}$. Trajectory sensitivity allows us to quantify the variation of the system trajectory caused by a small perturbation in system parameters.

Let us define the flows of $\boldsymbol{x}$ and $\boldsymbol{z}$ with time t as:

$$\boldsymbol{x(t)} = \boldsymbol{\psi_x}\left(\boldsymbol{x}, \boldsymbol{t}, \boldsymbol{\lambda}\right) \tag{4}$$

$$\boldsymbol{z(t)} = \boldsymbol{\psi_z}\left(\boldsymbol{x}, \boldsymbol{t}, \boldsymbol{\lambda}\right) \tag{5}$$

One can combine (2), (3) and (4), (5) for the initial conditions of $\boldsymbol{x(t)}$ and $\boldsymbol{z(t)}$ as:

$$\boldsymbol{\psi_x}\left(\boldsymbol{x_0}, \boldsymbol{0}, \boldsymbol{\lambda}\right) = \boldsymbol{x_0} \tag{6}$$

$$\boldsymbol{G}\left(\boldsymbol{x_0}, \boldsymbol{\psi_z}\left(\boldsymbol{x_0}, \boldsymbol{0}, \boldsymbol{\lambda}\right), \boldsymbol{\lambda}\right) = \boldsymbol{0} \tag{7}$$

The sensitivity of the flow $\boldsymbol{\psi_x}$ to the parameter variation $\boldsymbol{\lambda}$ can be obtained from Taylor series expansions of (4) as:

$$\boldsymbol{\Delta x(t)} = \frac{\boldsymbol{\partial \psi_x}\left(\boldsymbol{x_0}, \boldsymbol{t}, \boldsymbol{\lambda}\right)}{\boldsymbol{\partial \lambda}} \boldsymbol{\Delta \lambda} + \text{higher order terms.} \tag{8}$$

Considering higher-order terms can improve the accuracy, but introduces additional complexity. Therefore, it is a usual practice to use the truncated series of (8) containing the first-order terms, as such an approximation ensures sufficient accuracy. Neglecting higher-order terms and using (4), one can write:

$$\boldsymbol{\Delta x(t)} \approx \frac{\boldsymbol{\partial x(t)}}{\boldsymbol{\partial \lambda}} \boldsymbol{\Delta \lambda} = \boldsymbol{x_\lambda(t)} \boldsymbol{\Delta \lambda} \tag{9}$$

Similarly, for $\boldsymbol{z}$:

$$\boldsymbol{\Delta z(t)} \approx \frac{\boldsymbol{\partial z(t)}}{\boldsymbol{\partial \lambda}} \boldsymbol{\Delta \lambda} = \boldsymbol{z_\lambda(t)} \boldsymbol{\Delta \lambda} \tag{10}$$

The trajectory sensitivities $\boldsymbol{x_\lambda} = \frac{\boldsymbol{\partial x}}{\boldsymbol{\partial \lambda}}$ and $\boldsymbol{z_\lambda} = \frac{\boldsymbol{\partial z}}{\boldsymbol{\partial \lambda}}$ of the AC-MTDC grid can be derived by differentiating the DAEs given in (2) and (3) with respect to $\boldsymbol{\lambda}$:

$$\begin{aligned} \boldsymbol{\dot{x}_\lambda} &= \frac{\boldsymbol{\partial F}\left(\boldsymbol{t}\right)}{\boldsymbol{\partial x}} \boldsymbol{x_\lambda} + \frac{\boldsymbol{\partial F}\left(\boldsymbol{t}\right)}{\boldsymbol{\partial z}} \boldsymbol{z_\lambda} + \frac{\boldsymbol{\partial F}\left(\boldsymbol{t}\right)}{\boldsymbol{\partial \lambda}} \\ &\equiv \boldsymbol{F_x}\left(\boldsymbol{t}\right) \boldsymbol{x_\lambda} + \boldsymbol{F_z}\left(\boldsymbol{t}\right) \boldsymbol{z_\lambda} + \boldsymbol{F_\lambda}\left(\boldsymbol{t}\right) \end{aligned} \tag{11}$$

and

$$\begin{aligned} \boldsymbol{0} &= \frac{\boldsymbol{\partial G}\left(\boldsymbol{t}\right)}{\boldsymbol{\partial x}} \boldsymbol{x_\lambda} + \frac{\boldsymbol{\partial G}\left(\boldsymbol{t}\right)}{\boldsymbol{\partial z}} \boldsymbol{z_\lambda} + \frac{\boldsymbol{\partial G}\left(\boldsymbol{t}\right)}{\boldsymbol{\partial \lambda}} \\ &\equiv \boldsymbol{G_x}\left(\boldsymbol{t}\right) \boldsymbol{x_\lambda} + \boldsymbol{G_z}\left(\boldsymbol{t}\right) \boldsymbol{z_\lambda} + \boldsymbol{G_\lambda}\left(\boldsymbol{t}\right) \end{aligned} \tag{12}$$

Equations (11) and (12) form a new set of DAEs with new variables $\boldsymbol{x_\lambda}$ and $\boldsymbol{z_\lambda}$. Solving (2), (3) and (11), (12) simultaneously, we get $\boldsymbol{x}$, $\boldsymbol{z}$ and the sensitivities $\boldsymbol{x_\lambda}$ and $\boldsymbol{z_\lambda}$.

Remark I: If one uses implicit numerical integration techniques to solve (2), (3), then at each time-step the same Jacobian matrices be same as in (11), (12) are computed. Therefore, the only additional computation required for solving (11), (12) is forward and backward substitutions [26]. ■

In this work, a numerical approximation is utilized to find the sensitivities, which simplifies the implementation [26]. Using (9), (10) one can obtain the following approximated sensitivity

Copyright (c) 2019 IEEE. Personal use is permitted. For any other purposes, permission must be obtained from the IEEE by emailing pubs-permissions@ieee.org.

This is the author's version of an article that has been published in this journal. Changes were made to this version by the publisher prior to publication.
The final version of record is available at http://dx.doi.org/10.1109/TPWRS.2018.2890296

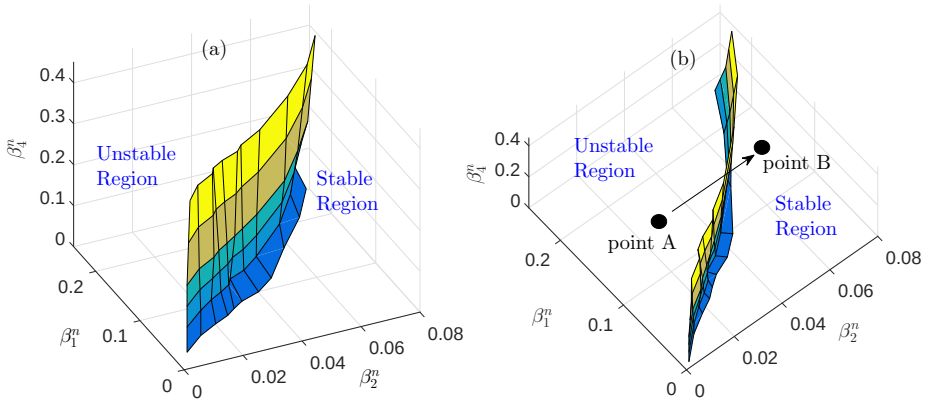

Fig. 6. Region of stability of the AC-MTDC grid following the outage of converter 3 (see Fig. 1). (a) Front view. (b) Top view. The critical values of β_2 are estimated through TSA while keeping β_1 and β_4 at constant values. Point A (unconstrained β_j) $\equiv$ ($\beta_1^n = 0.16$, $\beta_2^n = 0.025$, $\beta_4^n = 0.21$). Point B (constrained β_j) $\equiv$ ($\beta_1^n = 0.16$, $\beta_2^n = 0.075$, $\beta_4^n = 0.21$). Droop coefficients β are expressed in the unit of kV^2/MW.

function with respect to a scalar parameter λ:

$$\boldsymbol{x_\lambda} = \frac{\partial \boldsymbol{x}}{\partial \lambda} \approx \frac{\Delta \boldsymbol{x}}{\Delta \lambda} = \frac{\boldsymbol{\psi_x}\left(\boldsymbol{x_0}, t, \lambda + \Delta\lambda\right) - \boldsymbol{\psi_x}\left(\boldsymbol{x_0}, t, \lambda\right)}{\Delta \lambda} \quad (13)$$

$$\boldsymbol{z_\lambda} = \frac{\partial \boldsymbol{z}}{\partial \lambda} \approx \frac{\Delta \boldsymbol{z}}{\Delta \lambda} = \frac{\boldsymbol{\psi_z}\left(\boldsymbol{x_0}, t, \lambda + \Delta\lambda\right) - \boldsymbol{\psi_z}\left(\boldsymbol{x_0}, t, \lambda\right)}{\Delta \lambda} \quad (14)$$

This method involves two sets of simulations for two values of λ (e.g. λ_1 and λ_2). Trajectories of corresponding state vectors $\boldsymbol{x_1}$ and $\boldsymbol{x_2}$ are then computed. The sensitivities at λ_1 can be calculated as:

$$\boldsymbol{x_\lambda} \approx \frac{\boldsymbol{x_2} - \boldsymbol{x_1}}{\lambda_2 - \lambda_1} = \frac{\Delta \boldsymbol{x}}{\Delta \lambda} \quad (15)$$

Similarly, $\boldsymbol{z_\lambda}$ can also be found. If $\Delta\lambda$ is small, the numerical sensitivity is expected to be very close to the one from analytical methods. As highlighted in [26], this method is easier to implement compared to implicit integration along with forward and backward substitution. However, it is computationally more expensive.

2) Estimation of Stability Constraints for System Operators: In this work, we are interested in finding the stability constraints of the droop gain of a converter when multiple such converters are connected to the same AC grid. For example, AC grid #1 in Fig. 1 has converters #2 and #3 connected to it. Therefore, stability constraints for one of them is of interest following the outage of the other converter as it directly impacts the stability of AC grid #1. When a power system operates near the stability boundary, a small change in parameters results in large oscillations in sensitivity trajectories [25], which is much more significant than that of the system trajectories. The critical value is the theoretical value of a parameter that leads the power system trajectories into the stability boundary or moves the system to instability. The critical value can be used as the stability constraint for a parameter.

Nguyen *et al* in [27], proposed the Euclidean norm of the sensitivity vector as a measure of proximity to instability. The time-varying sensitivity norm with respect to parameter λ_k for an m-machine system is defined as:

$$S_{\lambda k}\left(t\right) = \sqrt{\sum_{i=1}^{m-1}\left(\frac{\partial \alpha_i\left(t\right)}{\partial \lambda_k}\right)^2 + \sum_{i=1}^{m}\left(\frac{\partial \omega_i\left(t\right)}{\partial \lambda_k}\right)^2} \quad (16)$$

where, α_i is the rotor angle of the i^{th} generator with respect to the reference angle of the AC grid and ω_i is its angular speed. For AC-MTDC grids with multiple asynchronous AC grids, the rotor angle of generators should be measured with respect to the reference angle defined for each AC grid. For the system shown in Fig. 1, rotor angle of G3, angle of bus 13, and angle of bus 14 are used as the references for AC grid #1, #2, and #3, respectively.

The inverse of the maximum value of the sensitivity norm $S_{\lambda k}$ is define as:

$$\eta = \frac{1}{\max\left(S_{\lambda k}\right)} \quad (17)$$

Ideally, at the point of instability:

$$\max(S_{\lambda k}) \rightarrow \infty \Rightarrow \eta \rightarrow 0 \quad (18)$$

Theoretically, $\eta = 0$ gives the stability constraint of the parameter λ_i. In this work, this parameter is chosen as the droop coefficient β_j of the converters, see Figs 3, 4. As discussed before, our focus will be on deriving the stability constraints of droop coefficients of converter #2 and #3. The steps involved in the proposed stability-constrained adaptive droop approach shown in Fig. 4 are as follows:

Step 1. The control center will be equipped with a detailed dynamic model of the AC-MTDC grid. This model should be an accurate representation of the actual system, which is run with initial states representing the present operating condition. The output of the state estimator is used to initialize the model.

Step 2. Different (N-1) credible contingency ('what if') simulations along with TSA are performed using the initialized dynamic model obtained in Step I. More specifically, outage of the critical converters (e.g. converters #2 and #3) are simulated. Next, the sensitivity norm given in (16) and corresponding η values (e.g., η_1 and η_2) for two different values of β_j (e.g., β_j^1 and β_j^2) are computed. Here, β_j is the droop coefficient of

Copyright (c) 2019 IEEE. Personal use is permitted. For any other purposes, permission must be obtained from the IEEE by emailing pubs-permissions@ieee.org.

This is the author's version of an article that has been published in this journal. Changes were made to this version by the publisher prior to publication.
The final version of record is available at http://dx.doi.org/10.1109/TPWRS.2018.2890296

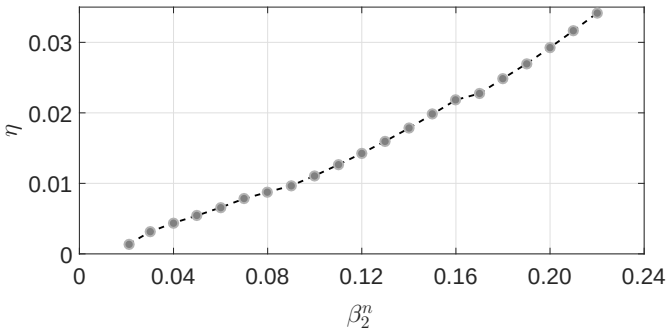

Fig. 7. Validation of the linearity between β and η.

the healthy converter, which would impact the stability of AC grid significantly. For these simulations the droop coefficient of all other converters are kept as constants. As an example, for the case of converter #2 outage, two different values of β_3 for converter #3 are used for obtaining η_1 and η_2. The values of β_1 and β_4 are kept constant during these computations.

Step 3. In this step, the stability constraints $\beta_j^{cr,est}$ are estimated using the extrapolation of the constructed straight line of β_j versus η curve and the intersection with the β_j-axis as shown in Fig. 5. For comment on linearity of η versus β_j curve near the stability boundary, see Remark II.

Step 4. Upon detection of a converter outage, impose the constraint $\beta_j^{cr,est}$ with some margin if the droop coefficient β_j violates it. Otherwise, let the unconstrained droop coefficients evolve. This is shown in Fig. 4(b). Detection of converter outage involves communication of detection signal to the control location, which could experience some latency. This delay should be taken into account while calculating the adaptive droop coefficient using the measured P_j shown in Fig. 4(a). It was shown in [33] that this latency can be calculated using time-stamp information at the sending end (i.e. the converter station) and the receiving end (i.e. the control center) assuming both are equipped with GPS antennas. If the computed latency is found to be τ, then the value of adaptive droop $\beta_j(t-\tau)$ will be enacted, where 't' is the instant when converter outage detection signal arrives at the control center. Impact of this delay will be studied later in this paper.

Note that only two simulations are required to compute β_j^{cr}, which makes the approach suitable for system operators.

3) Region of Stability in Multi-dimensional Droop Coefficient Space for Planners: During the planning studies, system planners would be interested in finding the region of stability in multi-dimensional droop coefficient space, which can act as operating guide for system operators during decision making. This can be done by repeating Steps 1 to 3 of the proposed approach for different values of β_1 and β_4. The process can be performed including different loading conditions as well (Fig. 4(c)).

Comment: It should be noted that the framework proposed in this paper is independent of the configuration (symmetric monopole, asymmetric bipole, and so on) and the topology (MMC vs 2-level) of the DC grids. It is also independent of the connectivity of the AC-MTDC grid.

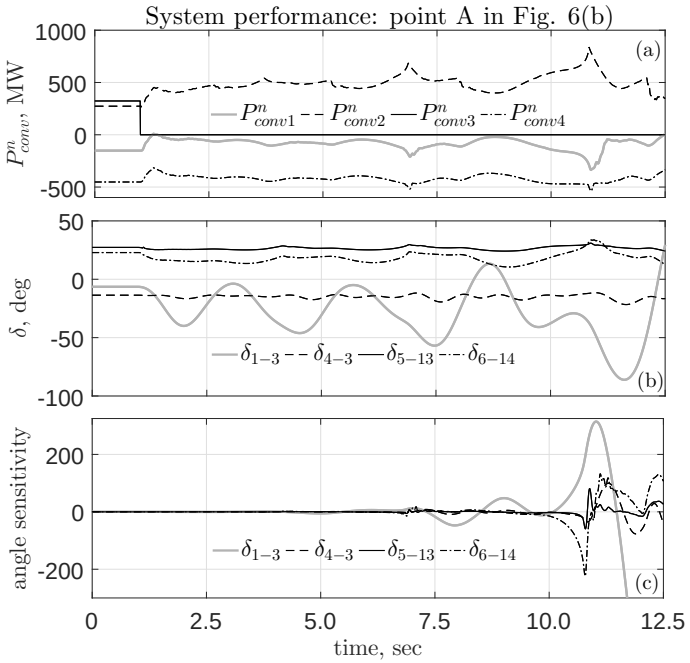

Fig. 8. Performance of the system following the outage of the negative pole converter of the converter station #3 in Fig. 1 with droop coefficients representing point A in Fig. 6(b). Angle sensitivity: $\frac{\partial \delta}{\partial \beta_2^n}$.

V. Results and Validation

The proposed approach is implemented in the test system shown in Fig. 1. In this paper, the outage of the negative pole converter of the converter stations are considered. To simulate the converter outage, both the DC-side and the AC-side breakers ($DCCB_n$ and $ACCB_n$ in Fig. 2) at the respective converter pole are opened. However, the DC cable connections to the switchyard of the affected converter is retained, which is the usual practice in an MTDC grid under $P - V_{dc}$ droop control with common pilot bus DC-link voltage [34]. This ensures a stable operation of the system in case of the outage of the converter station with the pilot bus. For all case studies, the droop gains of the positive pole converters are assumed to be equal to 0.1 pu kV^2/MW. The case study with outage of converter #3 is discussed next.

A. Case Study I: Converter # 3 Outage

For this case study, the real power loads at buses #9 and #10 are assumed to be 2000 MW each and the reference powers of converter #2 and #3 are considered as 650 MW and 550 MW, respectively. All the other relevant data are shown in Fig. 1. The region of stability of the AC-MTDC grid following the outage of converter #3 in (β_2^n, β_1^n, β_4^n) plane is shown in Fig. 6 in which Fig. 6(a) and Fig. 6(b) shows the front and the top view, respectively. Superscript 'n' stands for negative pole.

As explained earlier, to accomplish the region of stability in the multi-dimensional droop coefficient plane, Step 1 to Step 3 of the proposed stability-constrained adaptive droop approach are repeated for several sets of (β_1^n, β_4^n) combinations. For a given set of values of (β_1^n, β_4^n), it has been found that the stability constraint appear as a lower limit of β_2^n, which

Copyright (c) 2019 IEEE. Personal use is permitted. For any other purposes, permission must be obtained from the IEEE by emailing pubs-permissions@ieee.org.

This is the author's version of an article that has been published in this journal. Changes were made to this version by the publisher prior to publication.
The final version of record is available at http://dx.doi.org/10.1109/TPWRS.2018.2890296

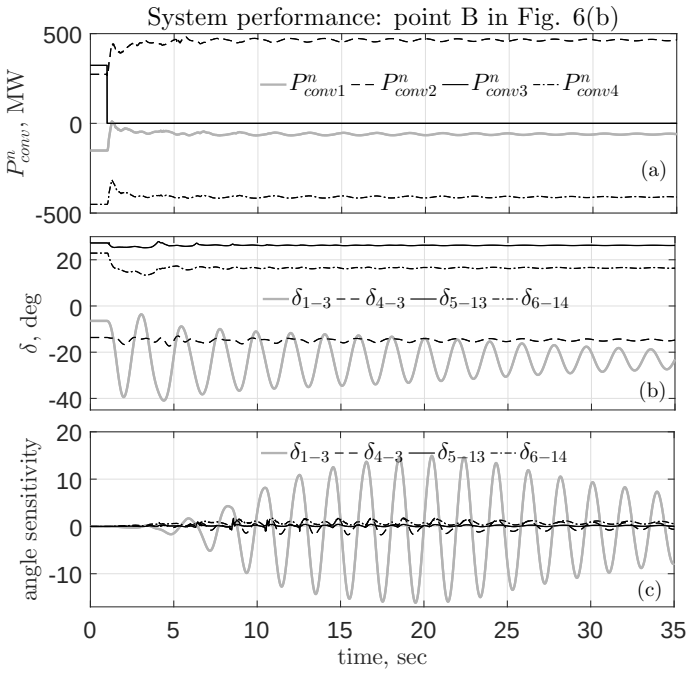

Fig. 9. Performance of the system following the outage of the negative pole converter of the converter station #3 in Fig. 1 with droop coefficients representing point B in Fig. 6(b). Angle sensitivity: $\frac{\partial \delta}{\partial \beta_2^n}$.

segregates the two regions as the stable region and the unstable region as shown in Fig. 6. The surface shown in Fig. 6 determines the critical values of the droop coefficients (β_1^n, β_2^n, and β_4^n) for a given operating condition following the outage of converter #3. One can call this surface as the 'critical surface' of the system. This critical surface can be used to impose constraints on the adaptive droop algorithm-

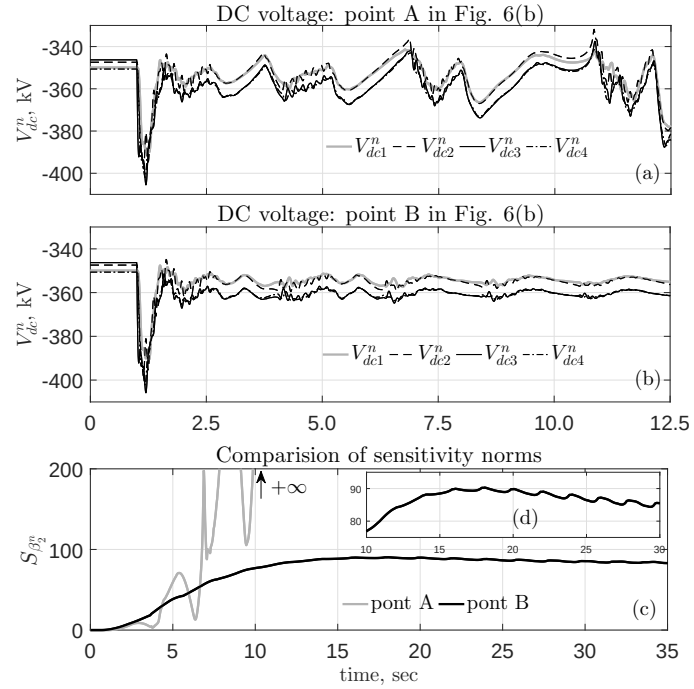

Fig. 10. Comparison of system performance following the outage of the negative pole converter of the converter station #3. DC voltages of negative poles corresponding to (a) point A in Fig. 6(b) and (b) point B in Fig. 6(b). (c) Comparison of sensitivity norms for points A and B. (d) Zoomed version of (c) during $t = 10 - 30$ s.

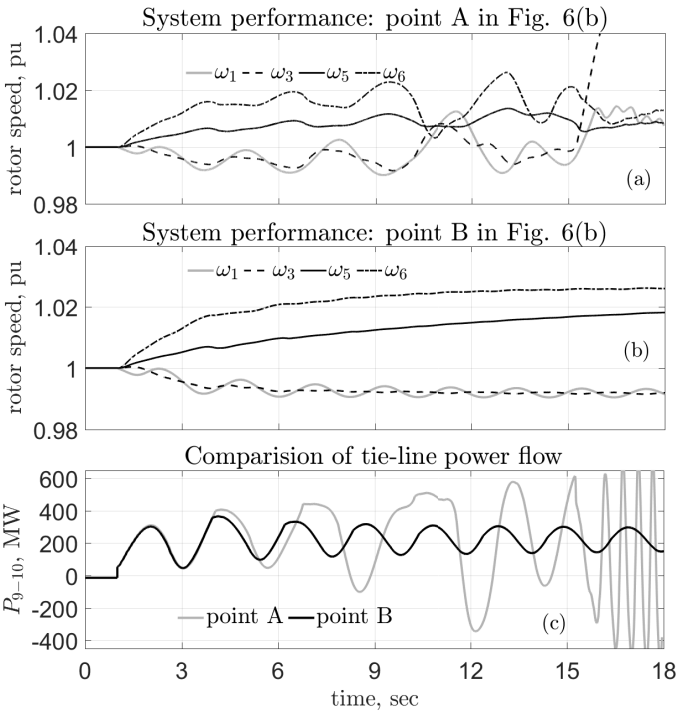

Fig. 11. Comparison of system performance following the outage of the negative pole converter of the converter station #3. Rotor speed of the synchronous machines corresponding to (a) point A in Fig. 6(b) and (b) point B in Fig. 6(b). (c) Comparison of tie-line power flow for points A and B.

based droop coefficients before the updating step (Fig. 4) as proposed in Section IV-A.

Remark II: Comment on selection of $\beta_2^{n,1}$ and $\beta_2^{n,2}$- Accurate estimation of the stability constraint in Step 3 is dependent on the assumption of linearity between η and β_2^n shown in Fig. 5. For numerous other applications of TSA, it has been found that η vs λ characteristic is approximately linear, especially in the vicinity of the stability boundary [27]. Figure 7 shows the variation of η versus β_2^n for this case study with a specific set of values for β_1^n and β_4^n. It can be observed that the relationship is piecewise linear in different ranges of β_2^n. Thus, the operators should choose two values $\beta_2^{n,1}$ and $\beta_2^{n,2}$ with input from operating guide prepared by system planners to obtain a reasonable estimate of β_2^{crit}.

1) Time-domain Simulation to Validate the Proposed Approach: To demonstrate the effectiveness of the proposed approach the following values of unconstrained droop coefficients are selected $\beta_1^n = 0.16$, $\beta_4^n = 0.21$, and $\beta_2^n = 0.025$, which correspond to point A in the unstable region of the 3-dimensional droop plane shown in Fig. 6(b). The performance of the AC-MTDC grid, following the outage of the negative pole of converter station #3 is shown in Fig. 8, which verifies that the system is unstable under this scenario.

It can be shown from the TSA that the critical value $\beta_2^{n,cr}$ corresponding to the set ($\beta_1^n = 0.16$, $\beta_4^n = 0.21$) is 0.065. Therefore, one can impose this constraint on β_2^n (i.e. the droop gain of the converter in the same AC grid, which would impact the stability of that AC grid significantly) with some margin as in Step 3, such that the point moves to the stable region (e.g. point B) as shown in Fig. 6. In other words if one can increase the value of β_2^n greater than the critical value without

Copyright (c) 2019 IEEE. Personal use is permitted. For any other purposes, permission must be obtained from the IEEE by emailing pubs-permissions@ieee.org.

This is the author's version of an article that has been published in this journal. Changes were made to this version by the publisher prior to publication.
The final version of record is available at http://dx.doi.org/10.1109/TPWRS.2018.2890296

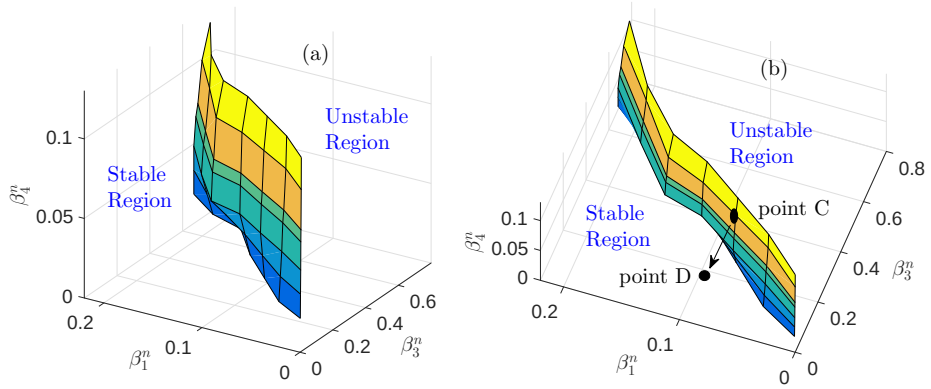

Fig. 12. Region of stability of the AC-MTDC grid following the outage of converter 2 (see Fig. 1). (a) Front view. (b) Top view. The critical values of β_3 are estimated through TSA while keeping β_1 and β_4 at constant values. Point C (unconstrained β_j, a point on the surface) $\equiv$ ($\beta_1^n = 0.1084$, $\beta_3^n = 0.298$, $\beta_4^n = 0.1007$). Point D (constrained β, a point in the stable region) $\equiv$ ($\beta_1^n = 0.1084$, $\beta_3^n = 0.1000$, $\beta_4^n = 0.1007$). Droop coefficients β are expressed in the unit of kV^2/MW.

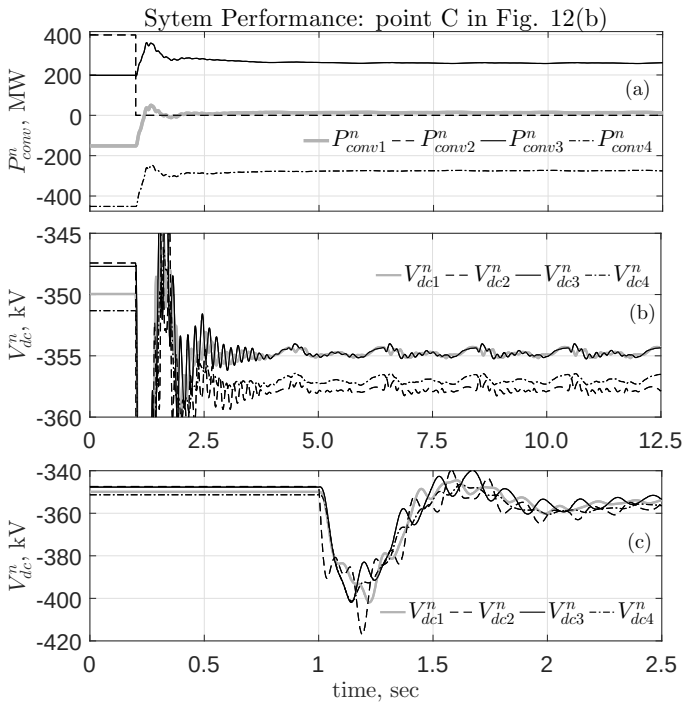

Fig. 13. System performance following the outage of the negative pole converter of the converter station #2 corresponding to point C in Fig. 12(b). (a) Converter power of negative poles. (b) DC voltages of negative poles. (c) Zoomed view of (b).

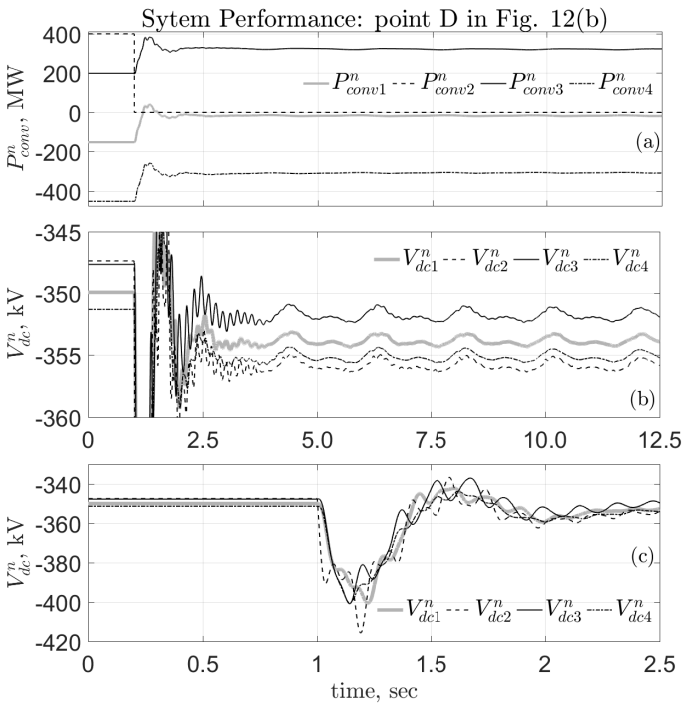

Fig. 14. System performance following the outage of the negative pole converter of the converter station #2 corresponding to point D in Fig. 12(b). (a) Converter power of negative poles. (b) DC voltages of negative poles. (c) Zoomed view of (b).

changing the values of β_1^n and β_4^n the system stability will be ensured. To demonstrate this, in this case study we select the droop coefficient values corresponding to point B: $\beta_1^n = 0.16$, $\beta_4^n = 0.21$, and $\beta_2^n = 0.075$. The time-domain simulation corresponding to this point is shown Fig. 9, which validates the effectiveness of the proposed approach.

Figures 10 and 11 compare the system performance following converter #3 outage corresponding to point A and point B. Generator speeds Fig. 11(a) and tie-line power in Fig. 11(b) show that the system operating at point A is unstable, whereas the corresponding responses from Figs 11 (b) and (c) confirm that point B is in the stable region. It can be seen from Fig. 10(c) that when the system is unstable the trajectory sensitivity norm reaches infinity, whereas it is finite for the case of stable system.

B. Case Study II: Converter # 2 Outage

For this case study, the real power loads at buses #9 and #10 are assumed to be 2050 MW and 1950 MW, respectively. The reference powers of converter #2 and #3 are considered as 800 MW and 400 MW, respectively. The same procedure as in Case Study I is followed here to derive the region of stability in the multi-dimensional droop coefficient plane following the outage of converter #2, which is shown in Fig. 12.

Copyright (c) 2019 IEEE. Personal use is permitted. For any other purposes, permission must be obtained from the IEEE by emailing pubs-permissions@ieee.org.

This is the author's version of an article that has been published in this journal. Changes were made to this version by the publisher prior to publication.
The final version of record is available at http://dx.doi.org/10.1109/TPWRS.2018.2890296

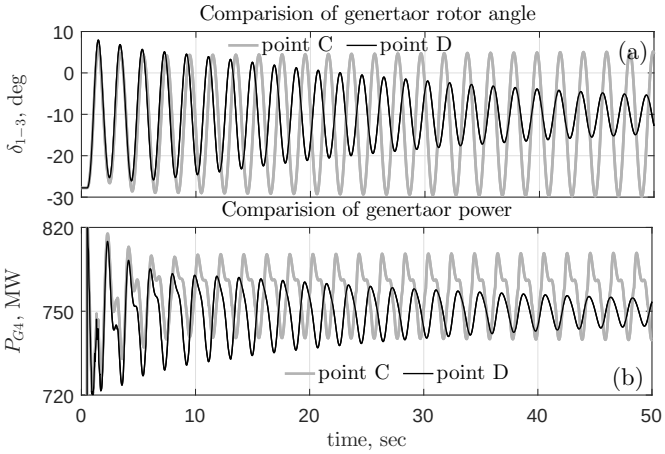

Fig. 15. Comparison of system performance following the outage of the negative pole converter of the converter station #2.

Unlike Case Study I, in this case study, it has been observed that for a given set of values of (β_1^n, β_4^n) the stability constraints appears as an upper limit of β_3^n and accordingly the region of stability can be defined, see Fig. 12.

1) Time-domain Simulation to Validate the Proposed Approach: To further validate the effectiveness of the proposed approach, in this case, the following combination of droop gains is selected for converters #1 and #4: $\beta_1^n = 0.1084$, $\beta_4^n = 0.1007$. For this combination of droop coefficients, TSA indicates that the stability constraint $\beta_3^{n,cr}$ is 0.298 (point C in Fig. 12(b), a point on the critical surface). The performance of the AC-MTDC grid, following the outage of the negative pole of converter station #2 is shown in Figs 13-15. It is interesting to note from Fig. 15 that the AC system operating at point C is marginally stable, even though it is not apparent from the DC-side response in Fig. 13.

To make the system stable, the value of β_3^n is reduced to 0.10 (point D in Fig. 12(b), a point in the stable region). The corresponding system response shown in Figs 14 and 15 further validates the effectiveness of the proposed approach.

C. Impact of DC Cable Model on the Proposed Approach

In the case studies I and II, a simplified DC cable model [28] was adopted. To evaluate the impact of the DC cable model, an improved approximation shown in Fig. 16 considered. This

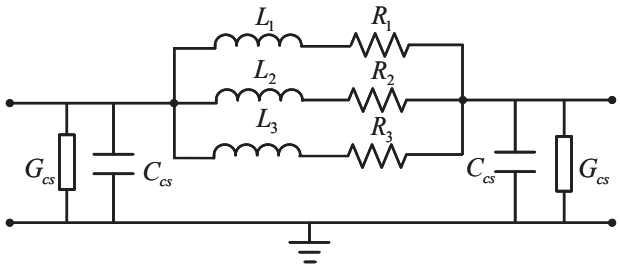

Fig. 16. Frequency dependent π model for DC cable [35].

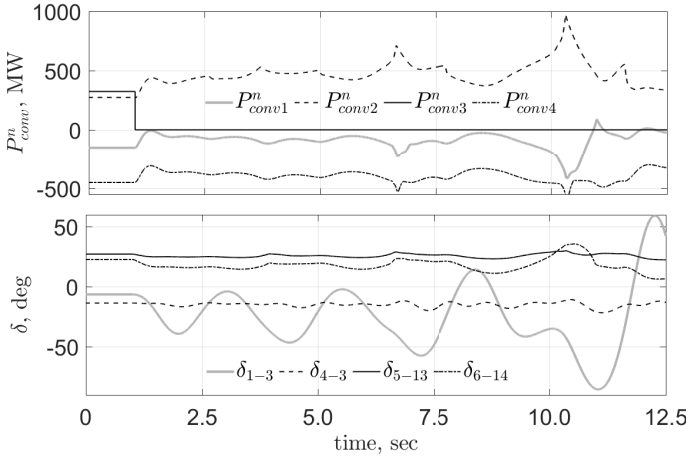

Fig. 17. System performance following the outage of the negative pole converter of the converter station #3 under unconstrained droop coefficients for the system with the frequency dependent π model for DC cables [35]. The droop coefficients are: $\beta_1^n = 0.16$, $\beta_4^n = 0.21$, and $\beta_2^n = 0.025$.

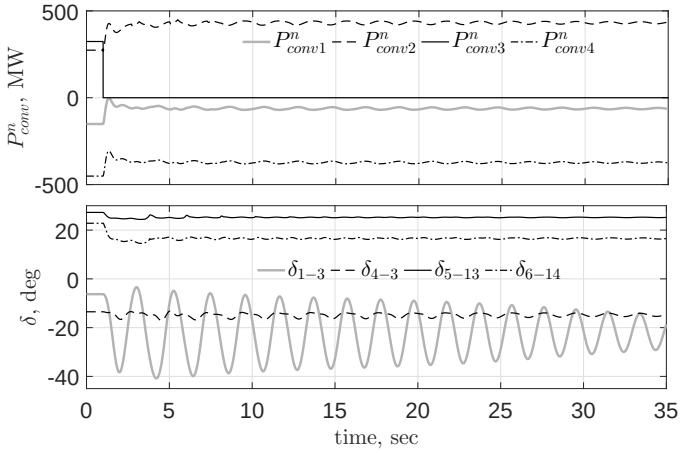

Fig. 18. System performance following the outage of the negative pole converter of the converter station #3 under stability-constrained droop coefficients for the system with the frequency dependent π model for DC cables [35]. The droop coefficients are: $\beta_1^n = 0.16$, $\beta_4^n = 0.21$, and $\beta_2^n = 0.10$.

cable model is known as the 'Fitted π' section model [35] since the parallel $R-L$ elements are calculated through a fitting algorithm to match the frequency response of a wide-band cable model [36]. The parameters of the cable model are given in the Appendix.

For this analysis, the same test system used in Case Study I is considered. As explained earlier, to find out the critical value of β_2^n following the outage of converter #3, Step 1 to Step 3 of the proposed stability-constrained adaptive droop approach are carried out for the set ($\beta_1^n = 0.16$, $\beta_4^n = 0.21$). It can be shown from the TSA that the critical value $\beta_2^{n,cr}$ corresponding to the this set is 0.080. It can be noted that the critical value for β_2^n under Case Study I (with the simple π model for the DC cable) for the same set ($\beta_1^n = 0.16$, $\beta_4^n = 0.21$) was 0.065.

Copyright (c) 2019 IEEE. Personal use is permitted. For any other purposes, permission must be obtained from the IEEE by emailing pubs-permissions@ieee.org.

This is the author's version of an article that has been published in this journal. Changes were made to this version by the publisher prior to publication.
The final version of record is available at http://dx.doi.org/10.1109/TPWRS.2018.2890296

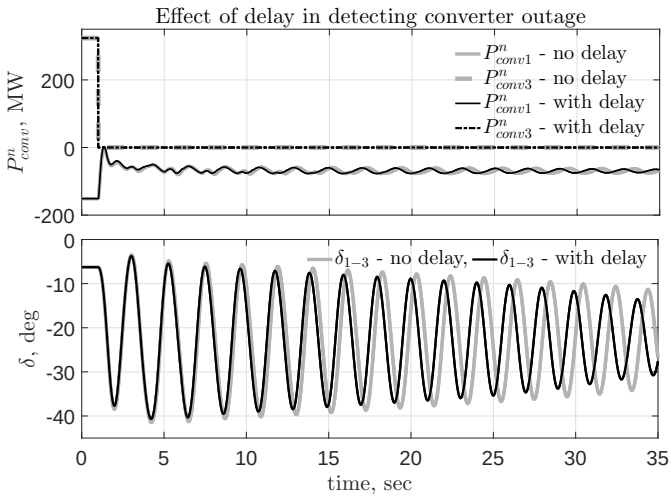

Fig. 19. Comparison of system performance following the outage of the negative pole converter of the converter station #3 with (500 ms) and without delay in the detection of converter outage.

1) Time-domain Simulation: The following values of unconstrained droop coefficients are selected $\beta^n_1 = 0.16$, $\beta^n_4 = 0.21$, and $\beta^n_2 = 0.025$, which correspond to point A shown in Fig. 6(b). The performance of the AC-MTDC grid, following the outage of the negative pole of converter station #3 is shown in Fig. 17, which verifies that the system is unstable under this scenario.

To make the system stable, the value of β^n_2 is increased to 0.10. The corresponding system response shown in Fig. 18 further validates the effectiveness of the proposed approach. This analysis demonstrates that the proposed stability-constrained adaptive droop approach gives expected results for the system, which considers advanced modeling of the DC cable.

2) Impacts of Possible Delays in Detecting Converter Outage: In Step 4 of the proposed approach described in Section IV, the possibility of delay in detecting converter outage and countermeasures for handling the same was elaborated. We consider a pessimistic scenario with delay of 500ms while typical latency in wide-area measurement systems in WECC Pacific DC Intertie ranges between 71 - 103ms [37]. To demonstrate the effect of the delay on the system dynamics, the following set of droop constants are selected: $\beta^n_1 = 0.16$, $\beta^n_4 = 0.21$, and $\beta^n_2 = 0.085$. Note that the value of β^n_2 is selected such that the system would operate very close to the stability margin, which could be more vulnerable in such scenarios. Figure 19 compares the dynamic performance of the system with and without delay in converter outage detection. The effectiveness of the proposed approach for handling such latencies is visible from the system response.

VI. Conclusion

A Trajectory Sensitivity Analysis (TSA)-based stability-constrained adaptive droop approach for autonomous power sharing following the outage of a converter in a MTDC grid is presented to ensure the stability of the surrounding AC systems, especially when two or more converters are connected to the same AC system. It was shown that the proposed approach can be a part of Dynamic Security Assessment (DSA) performed by the system operators. Nonlinear time-domain simulation results validate the effectiveness of the proposed method in an AC-MTCD grid consisting of three asynchronous AC grids and a four-terminal bipolar MTDC grid. The regions of stability of the system following two converter outage scenarios are presented in the multi-dimensional droop coefficient space, which can be derived by the system planners. Proposed TSA-based post-contingency analysis on these two outages under two loading conditions reveal that the stability constraint can appear either as an upper or as a lower limit on the droop coefficients.

Appendix: System Parameters

TABLE I
MTDC Grid Parameters

Symbol	Parameters	Values
V_{dc-nom}	Nominal DC-link voltage	$\pm$350 kV
R^p/R^n	Resistance of series AC filers	69.1 $m\Omega$
L^p/L^n	Inductance of series AC filers	38.8 mH
C^p_{dc}/C^n_{dc}	DC-bus capacitance of the converters	0.4 mF
R^p_{sc}/R^n_{sc}	Series resistance of C^p_{dc}/C^n_{dc}	1.0 $\mu\Omega$
R_g	DC grounding resistance	0.5 Ω
l	Length of the DC cables	400 km
R_p/R_n	Resistance of DC cables (π-model)	5.84 Ω
L_p/L_n	Inductance of DC cables (π-model)	1.29 H
C_p/C_n	Capacitance of DC cables (π-model)	55.0 μF
R_m	Resistance of the metallic return	5.84 Ω
L_m	Inductance of the metallic return	1.29 H
C_m	Capacitance of the metallic return	0.15 mF
K_{pI}	Proport. gain of inner control loop	$300R^{p/n}$
K_{iI}	Integral gain of inner control loop	$300L^{p/n}$
K_{pdc}	Proport. gain of DC voltage control	0.1 pu MW/kV^3
K_{idc}	Integral gain of DC voltage control	1.0 pu MW-s/kV^3

TABLE II
Parameters of Frequency Dependent DC Cable Model [38]

$R_1 = 1.1724 \times 10^{-1}$ Ω/km	$L_1 = 2.2851 \times 10^{-4}$ H/km
$R_2 = 8.2072 \times 10^{-2}$ Ω/km	$L_2 = 1.5522 \times 10^{-3}$ H/km
$R_3 = 1.1946 \times 10^{-2}$ Ω/km	$L_3 = 3.2942 \times 10^{-3}$ H/km
$C_{cs} = 1.9083 \times 10^{-11}$ F/km	$G_{cs} = 7.6333 \times 10^{-3}$ S/km

References

[1] CIGRE WG B4.52, *Feasibility of HVDC grids*. CIGRE technical brochure 533, Paris, April 2013.

[2] J. Liang, T. Jing, O. Gomis-Bellmunt, J. Ekanayake, and N. Jenkins, "Operation and control of multiterminal HVDC transmission for offshore wind farms," *IEEE Trans. on Power Delivery*, vol. 26, no. 4, pp. 2596–2604, Oct 2011.

[3] X. Lie, B. W. Williams, and Y. Liangzhong, "Multi-terminal DC transmission systems for connecting large offshore wind farms," in *IEEE Power and Energy Society General Meeting - Conversion and Delivery of Electrical Energy in the 21st Century*, 2008, pp. 1–7.

[4] X. Lie, Y. Liangzhong, and M. Bazargan, "DC grid management of a multi-terminal HVDC transmission system for large offshore wind farms," in *International Conference on Sustainable Power Generation and Supply*, 2009, pp. 1–7.

[5] N. R. Chaudhuri and B. Chaudhuri, "Adaptive droop control for effective power sharing in multi-terminal DC (MTDC) grids," *IEEE Trans. on Power Systems*, vol. 28, no. 1, pp. 21–29, Feb 2013.

Copyright (c) 2019 IEEE. Personal use is permitted. For any other purposes, permission must be obtained from the IEEE by emailing pubs-permissions@ieee.org.

This is the author's version of an article that has been published in this journal. Changes were made to this version by the publisher prior to publication.
The final version of record is available at http://dx.doi.org/10.1109/TPWRS.2018.2890296

[6] K. Rouzbehi, A. Miranian, A. Luna, and P. Rodriguez, "DC voltage control and power sharing in multiterminal DC grids based on optimal DC power flow and voltage-droop strategy," *IEEE Journal of Emerging and Selected Topics in Power Electronics*, vol. 2, no. 4, pp. 1171–1180, Dec 2014.

[7] M. A. Abdelwahed and E. F. El-Saadany, "Power sharing control strategy of multiterminal VSC-HVDC transmission systems utilizing adaptive voltage droop," *IEEE Trans. on Sustainable Energy*, vol. 8, no. 2, pp. 605–615, April 2017.

[8] J. Beerten and R. Belmans, "Analysis of power sharing and voltage deviations in droop-controlled DC grids," *IEEE Trans. on Power Systems*, vol. 28, no. 4, pp. 4588–4597, Nov 2013.

[9] X. Zhao and K. Li, "Adaptive backstepping droop controller design for multi-terminal high-voltage direct current systems," *IET Generation, Transmission Distribution*, vol. 9, no. 10, pp. 975–983, 2015.

[10] A. K. Marten, F. Sass, and D. Westermann, "Continuous p-v-characteristic parameterization for multi-terminal HVDC systems," *IEEE Trans. on Power Delivery*, vol. 32, no. 4, pp. 1665–1673, Aug 2017.

[11] C. Gavriluta, J. I. Candela, J. Rocabert, A. Luna, and P. Rodriguez, "Adaptive droop for control of multiterminal DC bus integrating energy storage," *IEEE Trans. on Power Delivery*, vol. 30, no. 1, pp. 16–24, Feb 2015.

[12] G. Li, Z. Du, C. Shen, Z. Yuan, and G. Wu, "Coordinated design of droop control in MTDC grid based on model predictive control," *IEEE Trans. on Power Systems*, no. 99, pp. 1–1, 2017.

[13] A. S. Abdel-Khalik, A. E. B. Abu-Elanien, A. A. Elserougi, S. Ahmed, and A. M. Massoud, "A droop control design for multiterminal HVDC of offshore wind farms with three-wire bipolar transmission lines," *IEEE Trans. on Power Systems*, vol. 31, no. 2, pp. 1546–1556, March 2016.

[14] H. Dong, Z. Xu, P. Song, G. Tang, Q. Xu, and L. Sun, "Optimized power redistribution of offshore wind farms integrated VSC-MTDC transmissions after onshore converter outage," *IEEE Trans. on Industrial Electronics*, vol. 64, no. 11, pp. 8948–8958, Nov 2017.

[15] W. Wang, Y. Li, Y. Cao, U. Häger, and C. Rehtanz, "Adaptive droop control of vsc-mtdc system for frequency support and power sharing," *IEEE Trans. on Power Systems*, vol. 33, no. 2, pp. 1264–1274, Mar. 2018.

[16] Y. Wang, W. Wen, C. Wang, H. Liu, X. Zhan, and X. Xiao, "Adaptive voltage droop control of multiterminal vsc-hvdc systems for dc voltage deviation and power sharing," *in early Access of IEEE Trans. on Power Delivery*, pp. 1–8, 2018.

[17] X. Chen, L. Wang, H. Sun, and Y. Chen, "Fuzzy logic based adaptive droop control in multiterminal HVDC for wind power integration," *IEEE Trans. on Energy Conversion*, vol. 32, no. 3, pp. 1200–1208, Sept 2017.

[18] Q. Shafiee, T. Dragičević, J. C. Vasquez, and J. M. Guerrero, "Hierarchical control for multiple DC-microgrids clusters," *IEEE Trans. on Energy Conversion*, vol. 29, no. 4, Dec 2014.

[19] S. Augustine, N. Lakshminarasamma, and M. K. Mishra, "Control of photovoltaic-based low-voltage dc microgrid system for power sharing with modified droop algorithm," *IET Power Electronics*, vol. 9, no. 6, pp. 1132–1143, 2016.

[20] S. Eren, M. Pahlevani, A. Bakhshai, and P. Jain, "An adaptive droop DC-bus voltage controller for a grid-connected voltage source inverter with LCL filter," *IEEE Trans. on Power Electronics*, vol. 30, no. 2, pp. 547–560, Feb 2015.

[21] A. Kirakosyan, E. F. El-Saadany, M. S. E. Moursi, S. S. Acharya, and K. A. Hosani, "Control approach for the multi-terminal HVDC system for the accurate power sharing," *IEEE Trans. on Power Systems*, vol. PP, no. 99, pp. 1–1, 2017.

[22] F. Thams, R. Eriksson, and M. Molinas, "Interaction of droop control structures and its inherent effect on the power transfer limits in multi-terminal VSC-HVDC," *IEEE Trans. on Power Delivery*, vol. 32, no. 1, pp. 182–192, Feb 2017.

[23] R. Eriksson, J. Beerten, M. Ghandhari, and R. Belmans, "Optimizing DC voltage droop settings for AC/DC system interactions," *IEEE Trans. on Power Delivery*, vol. 29, no. 1, pp. 362–369, Feb 2014.

[24] E. Prieto-Araujo, F. D. Bianchi, A. Junyent-Ferre, and O. Gomis-Bellmunt, "Methodology for droop control dynamic analysis of multiterminal VSC-HVDC grids for offshore wind farms," *IEEE Trans. on Power Delivery*, vol. 26, no. 4, pp. 2476–2485, Oct 2011.

[25] M. J. Laufenberg and M. A. Pai, "A new approach to dynamic security assessment using trajectory sensitivities," *IEEE Trans. on Power Systems*, vol. 13, no. 3, pp. 953–958, Aug 1998.

[26] I. A. Hiskens and M. Akke, "Analysis of the Nordel power grid disturbance of January 1, 1997 using trajectory sensitivities," *IEEE Trans. on Power Systems*, vol. 14, no. 3, pp. 987–994, Aug 1999.

[27] T. Nguyen, M. A. Pai, and I. A. Hiskens, "Sensitivity approaches for direct computation of critical parameters in a power system," in *International Journal of Electrical Power and Energy Systems*, vol. 24, 2002, pp. 337–343.

[28] N. R. Chaudhuri, B. Chaudhuri, R. Majumder, and A. Yazdani, *Multi-terminal Direct-Current Grids: Modeling, Analysis, and Control*. IEEE/John-Wiley, ISBN, Hoboken, NJ, USA, 2014.

[29] P. W. Sauer and M. A. Pai, *Power system dynamics and stability*. Upper Saddle River, N.J.: Prentice Hall, 1998.

[30] "IEEE recommended practice for excitation system models for power system stability studies - redline," *IEEE Std 421.5-2016 (Revision of IEEE Std 421.5-2005)*, pp. 1–453, Aug 2016.

[31] A. Yazdani and R. Iravani, *Voltage-sourced converters in power systems : modeling, control, and applications*. Hoboken, NJ, USA: Wiley, 2010.

[32] C. Schauder and H. Mehta, "Vector analysis and control of advanced static var compensators," *IET Proceedings on Generation, Transmission and Distribution*, vol. 140, no. 4, pp. 299–306, July 1993.

[33] N. R. Chaudhuri, S. Ray, R. Majumder, and B. Chaudhuri, "A new approach to continuous latency compensation with adaptive phasor power oscillation damping controller (POD)," *IEEE Trans. on Power Systems*, vol. 25, no. 2, pp. 939–946, 2010.

[34] B. Berggren, R. Majumder, C. Sao, and K. Lindén, "Method and control device for controlling power flow within a DC power transmission network," Assignee: ABB, Filed: 06/30/2010, US8553437 B2, issued Oct 08, 2013.

[35] J. Beerten, S. D'Arco, and J. A. Suul, "Frequency-dependent cable modelling for small-signal stability analysis of vsc-hvdc systems," *IET Generation, Transmission Distribution*, vol. 10, no. 6, pp. 1370–1381, 2016.

[36] ——, "Cable model order reduction for hvdc systems interoperability analysis," in *11th IET International Conference on AC and DC Power Transmission*, Feb 2015, pp. 1–10.

[37] B. J. Pierre, F. Wilches-Bernal, D. A. Schoenwald, R. T. Elliott, J. C. Neely, R. H. Byrne, and D. J. Trudnowski, "Open-loop testing results for the pacific dc intertie wide area damping controller," in *2017 IEEE Manchester PowerTech*, June 2017, pp. 1–6.

[38] S. Akkari, E. Prieto-Araujo, J. Dai, O. Gomis-Bellmunt, and X. Guillaud, "Impact of the dc cable models on the svd analysis of a multi-terminal hvdc system," in *2016 Power Systems Computation Conference (PSCC)*, June 2016, pp. 1–6.

Amirthagunaraj 'Raj' Yogarathinam (S'12) received the B.E. degree in electrical and electronic engineering from the University of Peradeniya, Sri Lanka, in 2013. He is currently pursuing the Ph.D. degree with the Pennsylvania State University, PA, USA. He was a Researcher and an Instructor with the Department of Electrical and Electronic Engineering, University of Peradeniya, from 2013 to 2014. He has also worked as a research intern at Argonne National Laboratory during summer 2018. His research interests include power system dynamics and control, MTDC, Hybrid-MTDC, wind power integration to the modern grid, wide-area monitoring and control, application of power electronics in power systems, online system identification, and smart grid.

Copyright (c) 2019 IEEE. Personal use is permitted. For any other purposes, permission must be obtained from the IEEE by emailing pubs-permissions@ieee.org.

This is the author's version of an article that has been published in this journal. Changes were made to this version by the publisher prior to publication.
The final version of record is available at http://dx.doi.org/10.1109/TPWRS.2018.2890296

Nilanjan Ray Chaudhuri (S'08-M'09-SM'16) received his Ph.D. degree from Imperial College London, London, UK in 2011 in Power Systems. From 2005-2007, he worked in General Electric (GE) John F. Welch Technology Center. He came back to GE and worked in GE Global Research Center, NY, USA as a Lead Engineer during 2011-2014. Presently, he is an Assistant Professor with the School of Electrical Engineering and Computer Science at Penn State, University Park, PA. He was an Assistant Professor with North Dakota State University, Fargo, ND, USA during 2014-2016. He is a member of the *IEEE* and *IEEE PES*. Dr. Ray Chaudhuri is the lead author of the book *Multi-terminal Direct Current Grids: Modeling, Analysis, and Control* (Wiley/IEEE Press, 2014), and an Associate Editor of the IEEE TRANSACTIONS ON POWER DELIVERY. Dr. Ray Chaudhuri is the recipient of the National Science Foundation Early Faculty CAREER Award in 2016.

Copyright (c) 2019 IEEE. Personal use is permitted. For any other purposes, permission must be obtained from the IEEE by emailing pubs-permissions@ieee.org.